© 2018. Published by The Company of Biologists Ltd | Journal of Cell Science (2018) 131, jcs212324. doi:10.1242/jcs.212324

RESEARCH ARTICLE

The Joubert syndrome protein ARL13B binds tubulin to maintain uniform distribution of proteins along the ciliary membrane

Ekaterina Revenkova[1,*], Qing Liu[1], G. Luca Gusella[2,3] and Carlo Iomini[1,3,4,5,‡]

ABSTRACT

Cilia-mediated signal transduction involves precise targeting and localization of selected molecules along the ciliary membrane. However, the molecular mechanism underlying these events is unclear. The Joubert syndrome protein ARL13B is a membrane-associated G-protein that localizes along the cilium and functions in protein transport and signaling. We identify tubulin as a direct interactor of ARL13B and demonstrate that the association occurs via the G-domain and independently from the GTPase activity of ARL13B. The G-domain is necessary for the interaction of ARL13B with the axoneme both *in vitro* and *in vivo*. We further show that exogenously expressed mutants lacking the tubulin-binding G-domain (ARL13B-ΔGD) or whose GTPase domain is inactivated (ARL13B-T35N) retain ciliary localization, but fail to rescue ciliogenesis defects of null *Arl13b*^{hnn} mouse embryonic fibroblasts (MEFs). However, while ARL13B-ΔGD and the membrane proteins Smoothened (SMO) and Somatostatin receptor-3 (SSTR3) distribute unevenly along the cilium of *Arl13b*^{hnn} MEFs, ARL13B-T35N distributes evenly along the cilium and enables the uniform distribution of SMO and SSTR3. Thus, we propose a so far unknown function of ARL13B in anchoring ciliary membrane proteins to the axoneme through the direct interaction of its G-domain with tubulin.

KEY WORDS: Primary cilia, Arl13b, Ciliopathies, Joubert syndrome, Ciliary membrane, Small GTPase, Tubulin, Axoneme

INTRODUCTION

Primary cilia are elongated protrusions of the cellular membrane where components of multiple signal transduction pathways concentrate to enable the response to a number of extracellular stimuli including chemicals, light and mechanical forces. Defects of ciliary structure or function cause systemic developmental abnormalities that are collectively called ciliopathies. A cilium is supported by a central core of nine or nine plus one microtubule doublets (A and B tubules) called the axoneme, which emanates from a modified centriole known as the basal body. The axoneme is sheathed by a ciliary membrane that, despite its continuity with the plasma membrane, displays a distinct protein and lipid composition reviewed by Emmer et al., 2010; Nachury et al., 2010.

The localization and arrangement of proteins along the ciliary membrane can vary greatly, ranging from ordered functional clusters that identify specific ciliary subdomains to even distribution along the length of the cilium (Fujiu et al., 2009; Huang et al., 2016; Iomini et al., 2006; Watnick et al., 2003; Zhang et al., 2013). Signaling molecules and structural components of the cilium are transported along the axonemal microtubules by specialized protein complexes, such as Bardet–Biedl syndrome (BBS) protein complex (BBSome) and the intraflagellar transport (IFT) motor proteins (Jin et al., 2010; Lechtreck, 2015; Piperno et al., 1996). Aberrant localization or accumulation of membrane proteins in the ciliary compartment can drastically interfere with the cilium signaling function (Dorn et al., 2012; Larkins et al., 2011). However, the mechanisms involved in the delivery, anchoring and segregation of proteins along the ciliary membrane are poorly understood.

Small GTPases contain a guanine-nucleotide-binding (G) site that alternates between an off (GDP-bound) and on (GTP-bound) state and function as molecular switches to control a number of intracellular processes, such as trafficking, cytoskeleton dynamics and signal transduction (Donaldson and Jackson, 2011). ADP ribosylation factor (Arf)-like proteins (Arls) ARL3, ARL4, ARL6 and Arl13B are members of the small GTPase Ras superfamily that localize to cilia, and function in cilia assembly and maintenance of axonemal architecture (Sung and Leroux, 2013). In particular, ARL13B – originally identified in genetic screenings as a protein essential for the integrity of ciliated organs and neural tube patterning – is a membrane-associated protein implicated in ciliary protein transport and signaling (Caspary et al., 2007; Larkins et al., 2011; Sun et al., 2004). In humans, mutations of *ARL13B* cause Joubert syndrome, a ciliopathy characterized by brain malformations, combined with polydactyly and renal cyst formation (Cantagrel et al., 2008; Thomas et al., 2015).

Although defective in size and structure, cilia persist in *Arl13b* mutants despite the fact that the compartmentalization of ciliary membrane proteins is disrupted, often resulting in aberrant accumulations along the ciliary membrane (Cevik et al., 2010; Larkins et al., 2011). Smoothened (SMO), together with the Patched-1 receptor (PATCH1) and Sonic Hedgehog ligand (SHH), is a main component of the Hedgehog (Hh) signaling pathway. In wild-type cells, SMO concentrates into the cilium and distributes along the ciliary membrane only upon binding of SHH to Patched. In contrast, in mouse embryonic fibroblasts (MEFs) derived from the homozygote *Arl13b*^{hnn} mouse allele, SMO is permanently present in the cilium and abnormally distributed in puncta along the ciliary membrane, regardless of the presence of SHH, thus impeding correct Hh signaling (Larkins et al., 2011; Mariani et al., 2016). Recently, it was shown that ARL13B acts as an effector of ARL3 through binding to the carrier proteins UNC119a/b and prenyl-binding protein phosphodiesterase 6D (PDE6D) to release prenylated or

[1]Department of Ophthalmology, Icahn School of Medicine at Mount Sinai, One Gustave L. Levy Place, New York, NY 10029, USA. [2]Department of Medicine, Icahn School of Medicine at Mount Sinai, One Gustave L. Levy Place, New York, NY 10029, USA. [3]Graduate School of Biomedical Sciences, Icahn School of Medicine at Mount Sinai, One Gustave L. Levy Place, New York, NY 10029, USA. [4]Department of Cell, Developmental and Regenerative Biology, Icahn School of Medicine at Mount Sinai, One Gustave L. Levy Place, New York, NY 10029, USA. [5]Friedman Brain Institute, Icahn School of Medicine at Mount Sinai, One Gustave L. Levy Place, New York, NY 10029, USA.
*Present address: Grail, 1525 O'Brien Drive, Menlo Park, CA 94025, USA.

‡Author for correspondence (carlo.iomini@mssm.edu)

C.I., 0000-0001-6483-9540

Received 24 October 2017; Accepted 23 March 2018

Journal of Cell Science (2018) 131, jcs212324. doi:10.1242/jcs.212324

myristoylated proteins such as nephrocystin-3 (NPHP3) and inositol polyphosphate-5-phosphatase E (INPP5E) specifically at the ciliary membrane (Gotthardt et al., 2015; Humbert et al., 2012; Zhang et al., 2016). Furthermore, absence of ARL13B leads to structural defects of axonemal microtubules (Caspary et al., 2007; Zhou and Anderson, 2010). Thus, the localization of ARL13B to cilia and its correct positioning along the cilium appear to be crucial for normal trafficking and distribution of membrane and lipidated proteins to the cilium, and for the maintenance of axonemal integrity. However, the factors that determine the correct localization of ARL13B within the cilium and the molecular interactions underlying its functions are currently unknown.

To gain mechanistic insight into ARL13B regulation and positioning along the ciliary membrane, we sought to identify interaction partners essential for its function in the cilium. Here, we show that the G-domain of ARL13B directly binds to tubulin, and that this binding is required for the even distribution of ARL13B along the ciliary membrane. Our findings indicate that, in addition to regulating IFT, ARL13B provides the means for the correct distribution of signaling proteins including SMO and somatostatin receptor 3 (SSTR3) along the ciliary membrane through interactions with the microtubules of the ciliary axoneme.

RESULTS

The G-domain of ARL13B interacts with tubulin

ARL13B includes an N-terminal amphipathic helix that is required for membrane insertion, followed by the G-domain, and an atypically elongated C-terminus that contains a coiled-coil domain and a proline-rich domain (PRD). The murine and human amino acid (aa) sequence of ARL13B show 80% identity, the most conserved regions spanning the G-domain and the C-terminus. To enhance the discovery of ARL13B interactors with these regions, we generated an antibiotic-selectable lentiviral vector that constitutively expresses murine ARL13B fused to a tandem affinity purification (TAP) tag (GFP-TEV-S-tag) at its N-terminus in cells of the immortalized human retinal pigment epithelium (hTERT-RPE1) cell line (Fig. S1A). Following transduction of hTERT-RPE1 and antibiotic selection, we isolated a cell line in which recombinant GFP-S-mARL13B and endogenous ARL13B were expressed at comparable levels and similarly located in the cilium (Fig. S1B,C). Cells of the selected line were grown to confluency, and ciliogenesis was induced by serum withdrawal. By using the TAP procedure (see Materials and Methods), cells were used to prepare a protein extract and isolate ARL13B-interacting proteins (Fig. 1A). The resulting set of proteins was separated by gel electrophoresis and the composition of the bands visible after silver staining was determined by mass-spectrometry (Fig. 1A).

In agreement with previous reports, we identified myosin and actin among the proteins interacting with the tagged ARL13B (Barral et al., 2012; Casalou et al., 2014). However, the most abundant proteins that, on the basis of band intensity and number of unique peptides, co-purified with TAP-tagged ARL13B were α- and β-tubulin with 137 and 238 peptides recovered, respectively (Fig. 1A,B). Specifically, the analysis of an ∼50 kDa band excised from a preparative gel included the following tubulin isotypes: tubulin beta chain (TUBB), 23 unique peptides; tubulin alpha-1B chain (TUBA1B), 17 unique peptides; tubulin beta-6 chain (TUBB6), 9 unique peptides; tubulin beta-2A chain (TUBB2A), 6 unique peptides; tubulin beta-4B chain (TUBB4B), 5 unique peptides; tubulin alpha-4A chain (TUBA4A), 3 unique peptides; tubulin beta-3 chain (TUBB3), 3 unique peptides. We corroborated the association of tubulin with ARL13B by immunoprecipitation of endogenous ARL13B from HEK293 cells, using a specific antibody against human ARL13B and detection of tubulin (Fig. 1C). These experiments not only confirmed the interaction between ARL13B and tubulin but also indicated overlapping activity of human and murine ARL13B.

Next, we asked if the interaction with tubulin depends on ARL13B binding GDP or GTP. GST fused to ARL13B (GST-ARL13B) immobilized on GSH sepharose beads was loaded with GDP or the non-hydrolysable analog GTPγS and then incubated with hTERT-RPE1 cell lysate. Similar amounts of tubulin co-precipitated with ARL13B regardless of its GDP or GTP bound form (Fig. 1D, lanes 2 and 3). We then analyzed tubulin binding using purified GST-ARL13B with the point mutation R79Q. The diseases-causing R79Q mutation in ARL13B has been shown to reduce ARL13B binding to GTP and to affect protein conformation in the GTP-bound state in the corresponding *Chlamydomonas* ARL13B mutant (Cantagrel et al., 2008; Miertzschke et al., 2014). Tubulin binding of GST-ARL13B in the presence of GTPγS was not affected by the mutation (Fig. 1D, lanes 2 and 4), thus, confirming that interaction between ARL13B and tubulins is not altered by ARL13B being bound to GTP or GDP binding state. However, tubulin molecules interacting with ARL13B appeared to be acetylated (Fig. 1D) and further investigation will be required to determine whether this acetylation is necessary for the interaction to occur.

To distinguish between a direct or indirect association of ARL13B with tubulin, we isolated recombinant GST-tagged human ARL13B from *E. coli* and incubated it in the presence of purified bovine brain tubulin. Incubation of the GST protein tag with tubulins was used as control. Glutathione (GSH) sepharose beads were added to each reaction mix to purify GST-ARL13B or control GST, and their interacting proteins were analyzed by western blotting. Tubulin was found in the eluate from the beads loaded with GST-ARL13B, but not in that from control GST (Fig. 2A and B, lanes 'GST-ARL13B aa 1-428' and 'GST'), thus indicating that ARL13B can directly interact with tubulin dimers. To map the tubulin-interacting regions of ARL13B, we purified a series of GST-fused fragments of ARL13B and a deletion mutant that lacks the G-domain while retaining the N-terminal amphipathic helix (Fig. 2A). GST pull-down of the mutants incubated with hTERT-RPE1 extract revealed that the G-domain and G-domain fragments that had been most truncated (aa 20–119 and aa 20–79), but not the coiled-coil region or the amphipathic helix, mediated the interaction with soluble tubulin (Fig. 2A-E). We have also examined tubulin binding with GST-ARL13B carrying the point mutation T35N located in a motif referred to as P-loop, which is highly conserved among GTP-binding proteins. The mutation of the corresponding Ser^{17} in Ras proteins (Ras S17N) affects their GTPase activity, and significantly interferes with Ras signaling by strongly altering Ras affinity to nucleotides and guanine-nucleotide exchange factors (GEFs) (Cool et al., 1999; Dascher and Balch, 1994; Feig, 1999). The T35N ARL13B mutation, which has been previously shown to render ARL13B non-functional (Duldulao et al., 2009; Humbert et al., 2012), did not hinder binding to tubulin (Fig. 2F), thus confirming that, at least *in vitro*, the interaction with tubulin does not depend on ARL13B GTPase activity.

The G-domain of ARL13B is not required for transport to the cilium but is necessary to control ciliary length and assembly

To investigate the cellular function of the tubulin-binding region, we created lentiviral vectors to express GFP-tagged deletion mutants of ARL13B in MEFs obtained from wild-type mice and from the Arl13b-null hennin *Arl13b*$^{hnn/hnn}$ (*Arl13b*^{hnn}) mice (Fig. 3 and

Journal of Cell Science (2018) 131, jcs212324. doi:10.1242/jcs.212324

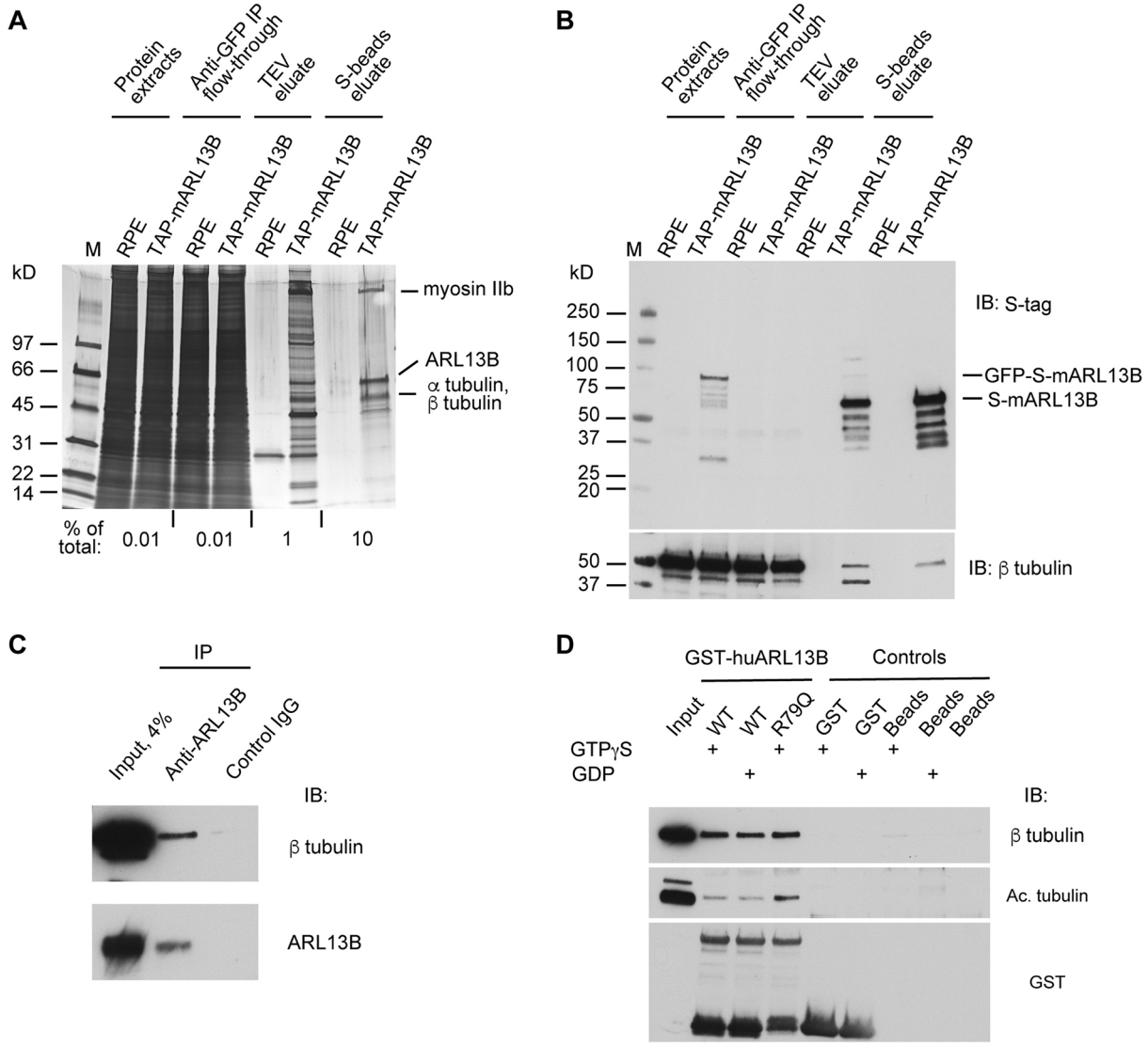

Fig. 1. ARL13B interacts with tubulin. (A,B) Identification of tubulin as an ARL13B-interacting protein by tandem affinity purification (TAP) and mass spectrometry (MS). (A) Silver-stained gel and (B) western blot analysis of purified fractions. (C) Co-immunoprecipitation of tubulin from HEK293 cell lysate after pull-down with anti-ARL13B antibody. (D) GST pull-down of recombinant GST-tagged human ARL13Bwt or GST-ARL13B R79Q after incubation with hTERT-RPE1 cell lysates. Note that ARL13B-interacting tubulin includes acetylated tubulin.

Fig. S2). Because the interaction with tubulin was mapped within the G-domain of ARL13B, we first asked whether the G-domain is required to translocate ARL13B to the ciliary compartment. As ARL13B interactions with the membrane through palmitoylation or myristoylation at the N-terminus are critical for its compartmentalization (Cevik et al., 2010; Duldulao et al., 2009; Hori et al., 2008; Larkins et al., 2011; Zhou and Anderson, 2010), we maintained the N-terminal amphipathic helix (aa 1–19) in our constructs (Fig. 3A). In agreement with Nozaki et al. (2017), we found that the chimeric proteins GFP-mARL13BΔGD, which lacks the GTPase domain (aa 20–198), and GFP-mARL13B T35N, which contains the T35N mutation predicted to disrupt the GTP-binding site, efficiently translocated to the cilium of hTERT-RPE1 cells (Fig. S2) as well as wild-type and *Arl13b*^{hnn} MEFs (Fig. 3D). In contrast, despite the presence of the complete G-domain with the ciliary localization motif RVxP (in which x denotes any aa) (Deretic et al., 2005; Geng et al., 2006; Ward et al., 2011), GFP-mARL13BΔCC that lacks the coiled-coil domain (aa 199–353) failed to localize to the cilium of hTERT-RPE1 cells (Fig. S2). Thus, the C-terminal domain, but not the G-domain, plays an essential role in ARL13B translocation into the ciliary compartment. However, the cilium-localized GFP-mARL13BΔGD could not restore the ciliary localization of the membrane-associated protein INPP5E in *Arl13b*^{hnn} MEFs (Fig. S3), suggesting an active role of the G-domain in INPP5E translocation into cilia (Nozaki et al., 2017).

Several studies in different species and cell types have shown that the overexpression of ARL13B causes cilium elongation (Hori et al., 2008; Larkins et al., 2011). To determine whether this effect depends on the G-domain, we transduced wild-type MEFs with constructs expressing GFP-ARL13B wild-type or GFP-ARL13B containing a mutated G-domain. Cilia length in most non-transduced MEFs was in the range of 2.0–2.9 µm (56.7% of cells) and 3.0–3.9 µm (33.3% of cells), whereas in GFP-mARL13B- or GFP-huARL13B-transduced MEFs the GFP-positive cilia were in the range of 5.0–5.9 µm and extended over 8.0 µm in 30.2% or 3.8% of the cells, respectively (Fig. 3B,D and E). Expression of

Journal of Cell Science (2018) 131, jcs212324. doi:10.1242/jcs.212324

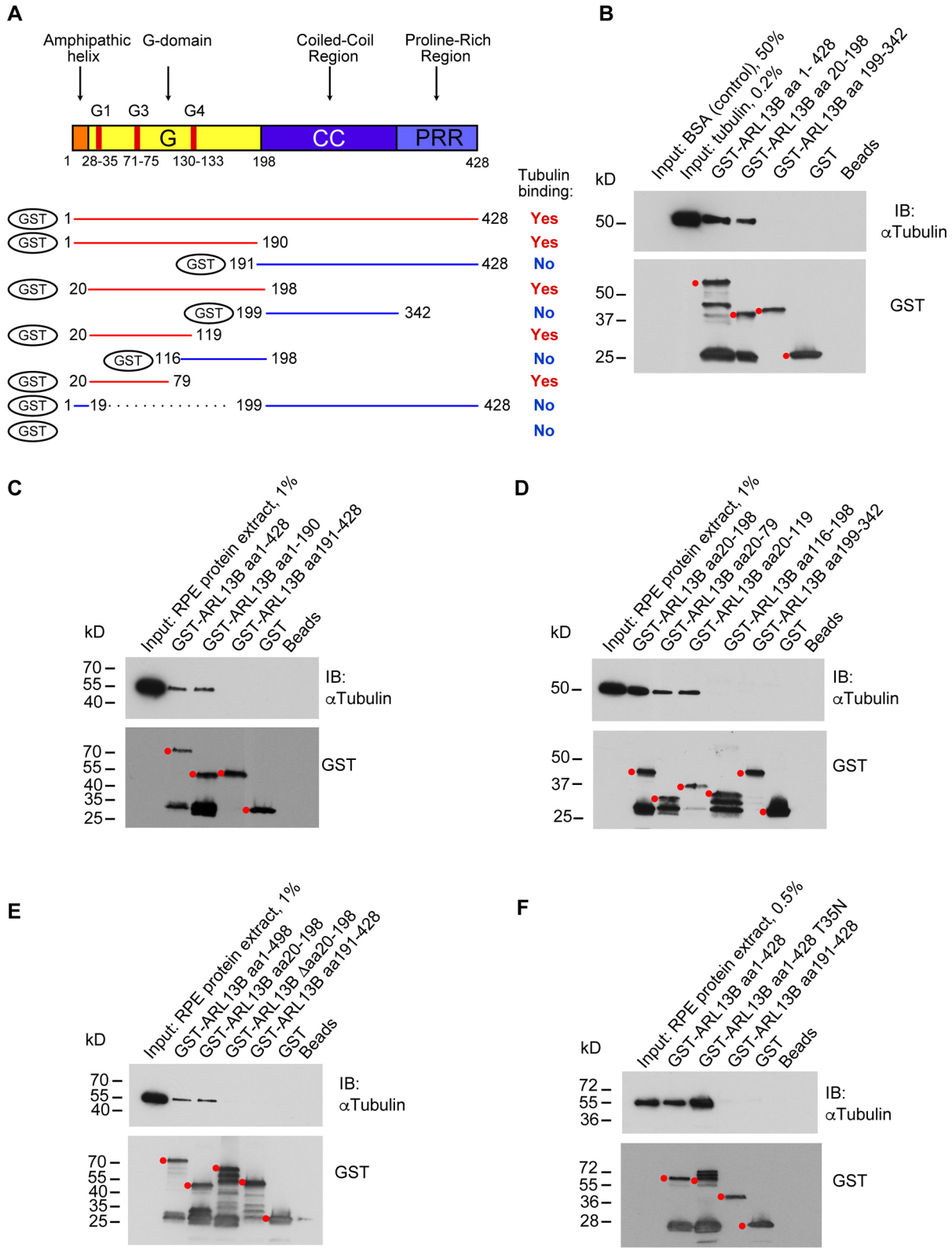

Fig. 2. The G-domain of ARL13B contains a tubulin-interacting region. (A) Schematic representation of the main domains of the ARL13B protein (top) and GST-fused fragments of ARL13B (bottom) purified from *E. coli*. (B) GST pull-down from a solution of purified tubulin dimer. (C-F) GST pull-down from hTERT-RPE1 cell lysate. Bands corresponding to fusion proteins of the expected size are marked with red dots; degradation products run below.

GFP-mARL13BΔGD or GFP-ARL13B T35N led to a comparable increase in cilia length (Fig. 3D and E) indicating that abnormal elongation of cilia does not depend on the presence of the G-domain.

Given that ectopic expression of the mARL13BΔGD mutant or wild-type mARL13B could similarly affect ciliary length, we asked whether the mARL13BΔGD mutant can rescue cilia length

Journal of Cell Science (2018) 131, jcs212324. doi:10.1242/jcs.212324

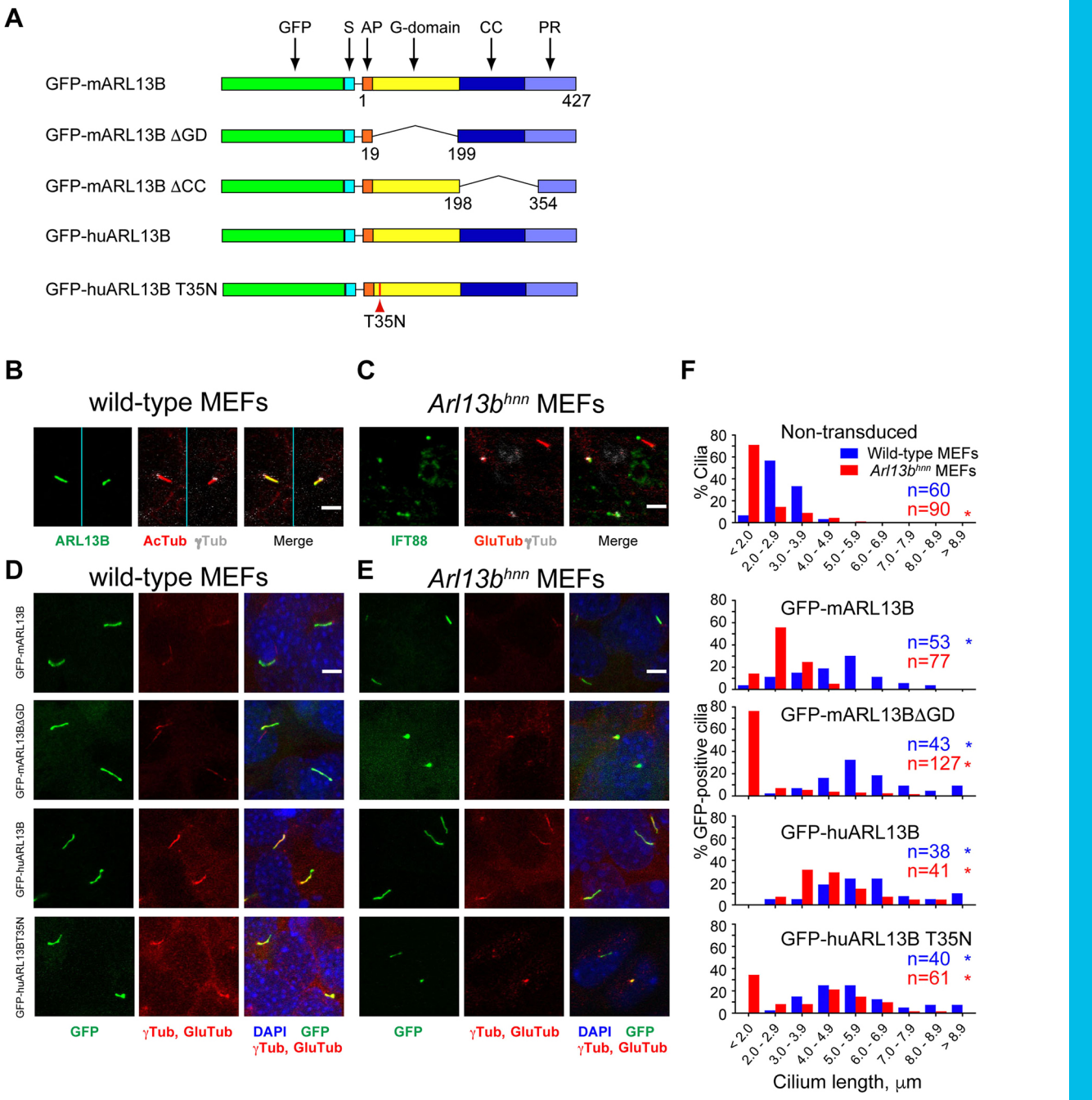

Fig. 3. ARL13B G-domain is dispensable for cilium localization but essential for cilium length regulation. (A) Domain structure of GFP-tagged wild-type and mutated ARL13B proteins expressed in mammalian cells as GFP fusions. (B-E) Cilia lengths in wild-type MEFs (B,D) and *Arl13b*^{hnn} MEFs (C,E) untransduced (B,C) or transduced with the indicated lentiviral expression vectors (D,E) were determined following immunofluorescence for ARL13B, acetylated tubulin and γ-tubulin in wild-type MEFs (B), IFT88, acetylated tubulin and γ-tubulin (C), and GFP, glutamylated tubulin and γ-tubulin (D,E). Nuclei were stained with DAPI. (F) Quantification of changes in cilia length distribution in wild-type and *Arl13b*^{hnn} MEFs expressing GFP-tagged ARL13B constructs compared to non-transduced controls. χ^2-test, **P*<0.0001 from non-transduced wild-type MEFs. *n*=number of cilia measured in two independent experiments. Scale bars: 5 µm.

and/or cilia assembly defect in ARL13B-null *Arl13b*^{hnn} MEFs (Caspary et al., 2007; Larkins et al., 2012). For accurate evaluation of cilia length, we measured cilia length of transduced *Arl13b*^{hnn} MEFs by co-staining with IFT88, which concentrates at the base and at the tip of the cilium, and in puncta along the cilia length, and with γ-tubulin to mark the basal body (see Materials and Methods) (Fig. 3C). In untransduced or GFP-mARL13BΔGD-transduced *Arl13b*^{hnn} MEFs, IFT subunits of complex B (IFT88) or complex A (IFT140), accumulated at the ciliary tip, (Fig. S4), consistent with results from Nozaki et al. (Nozaki et al., 2017). The majority of *Arl13b*^{hnn} MEFs cilia (71.1%) measured <2 µm (Fig. 3C,F), although some cilia >4 µm (5.5%) were also present (Fig. 3F). However, the ectopic expression of GFP-tagged wild-type mARL13B or huARL13B re-established a cilia length of most *Arl13b*^{hnn} MEFs to be 2.0–4.0 µm (Fig. 3E,F) (Larkins et al., 2011). In contrast, GFP-

Journal of Cell Science (2018) 131, jcs212324. doi:10.1242/jcs.212324

mARL13BΔGD failed to rescue the blunted cilia phenotype of *Arl13b*^{hnn} MEFs in the absence of the endogenous ARL13B (75% of cells with cilia <2 µm) (Fig. 3E,F). The ARL13B mutant containing the T35N point mutation in the G-domain, which maintains it in the non-functional GDP-locked state without affecting ARL13B-tubulin binding, was similarly unable to fully rescue the short cilia of *Arl13b*^{hnn} MEFs. However, 66% of cilia were >2 µm, suggesting that in cilium elongation GFP-ARL13B T35N is more efficient than mARL13BΔGD (Fig. 3E,F). These results support the idea that, although GTPase activity is necessary for the normal assembly and maintenance of the cilium, the G-domain of ARL13B harbors sequences with distinct functions that are important for cilia elongation.

The ARL13B G-domain sequence, but not its GTPase activity, is required to establish and maintain uniform distribution of ARL13B and other membrane proteins along the ciliary membrane

Although the majority of *Arl13b*^{hnn} MEFs displayed very short cilia we found that a small percentage of cells (~5%) were able to assemble a cilium with an axoneme that equaled or exceeded the length of cilia detected in wild-type MEFs (Fig. 3E). Because in *Arl13b*^{hnn} MEFs the membrane protein SMO was reported to aberrantly accumulate in discrete regions of the cilium and predominantly at the ciliary tip (Larkins et al., 2011), we carefully analyzed the distribution of the GFP-mARL13B and the GFP-mARL13BΔGD along the cilium of normal and *Arl13b*^{hnn} MEFs

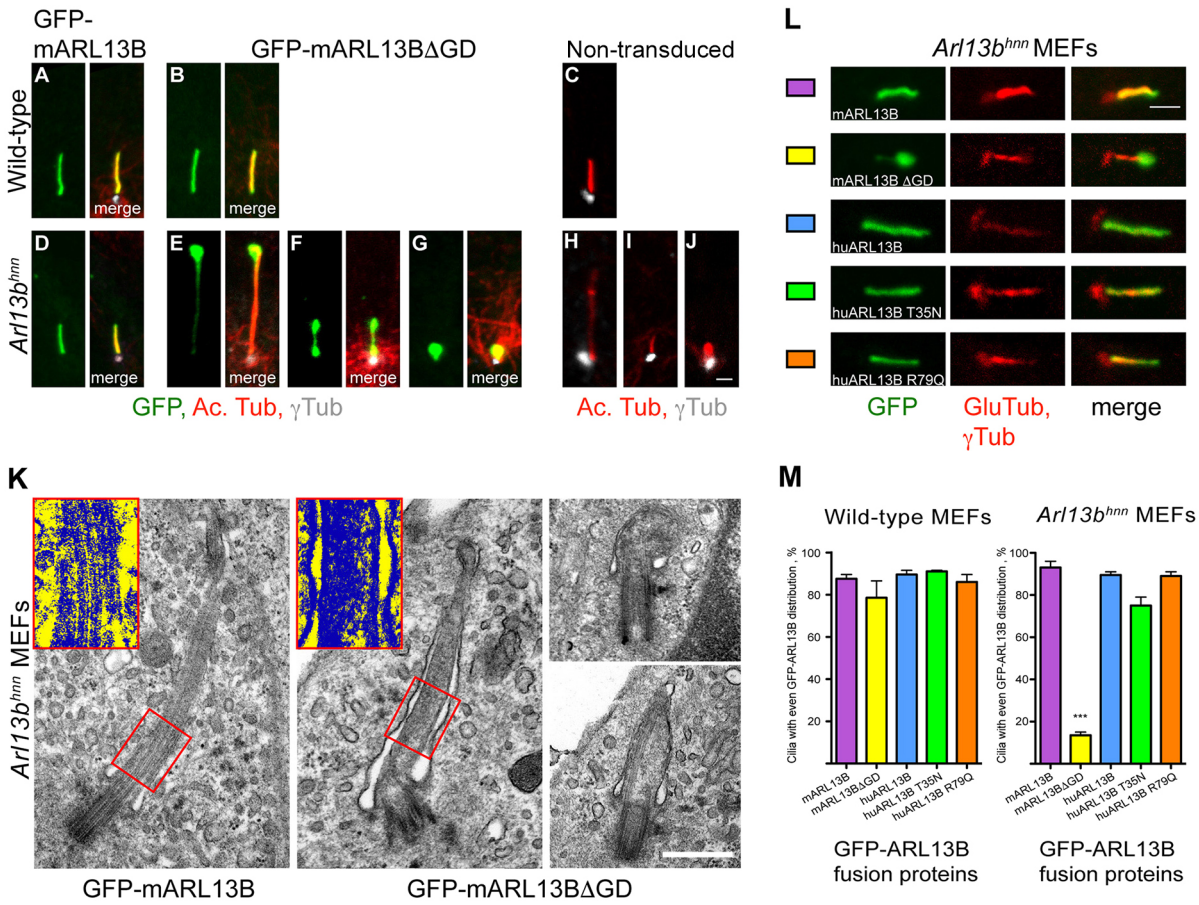

Fig. 4. The G-domain regulates ARL13B distribution along cilia. (A-J) Immunofluorescence of clonal *Arl13b*^{hnn} and wild-type MEFs untrasduced or expressing GFP-mARL13B, GFP-mARL13BΔGD (see Fig. S4A for expression levels of GFP-tagged variants of Arl13b). GFP, green, acetylated tubulin, red and γ-tubulin, white. (A,B) GFP-mARL13B and GFP-mARL13BΔGD uniformly distribute along cilia of wild-type MEFs. (C) Cilium of untransduced MEFs. (D) Ectopic GFP-mARL13B rescues the ciliary length defect and distributes uniformly along the ciliary membrane of *Arl13b*^{hnn} MEFs. (E,G) Ectopic GFP-mARL13BΔGD accumulates at the distal end (E) or at both ends (F) of cilia and in stump-like structures (G) of *Arl13b*^{hnn} MEFs but, it is dramatically reduced between cilia extremities (E and F). (K) Ultrastructural analysis by TEM of longitudinal sections of cilia of *Arl13b*^{hnn} MEFs. Clonal *Arl13b*^{hnn} MEFs transduced with GFP-mARL13BΔGD show accumulation of electron-dense deposit along the length of cilia (middle panel) and in stump-like structures (right panels). In contrast, clonal *Arl13b*^{hnn} MEFs transduced with GFP-mARL13B show no electron-dense accumulation along the cilia (left panel). Insets in K are gradient maps of the boxed areas. Note that axonemal microtubules (vertical yellow streaks) are visible in the cilium of *Arl13b*^{hnn} MEFs transduced with GFP-mARL13B, but not in the cilium of those transduced with GFP-mARL13BΔGD, which are mostly filled with electron-dense material (blue granules). (L) Color-coded examples of variable distribution of GFP-tagged ARL13B mutants along cilia of transduced *Arl13b*^{hnn} MEFs quantified in (M). Only the mGFP-ARL13BΔGD mutant lacking the G-domain aa sequence fails to distribute uniformly along the ciliary membrane of *Arl13b*^{hnn} MEFs. Wild-type and mutant ARLS13B carrying a single aa substitution affecting the GTPase active site uniformly distribute along the ciliary length. (M) Quantification of the distribution of GFP-tagged proteins in cilia of wild-type and *Arl13b*^{hnn} MEFs expressing GFP-tagged ARL13B constructs as indicated below the graph. Bars show percentage of cilia with even distribution of GFP-ARL13B proteins along the cilium (mean of two independent experiments, total number of cilia per experiment per construct was between 70 and 385, error bars represent standard error of the mean). In *Arl13b*^{hnn} MEFs, the difference between mARL13BdeltaGD and all other groups is significant (***P<0.001, one-way ANOVA with Tukey post-test for pairwise comparisons). Scale bars: 2 µm (J,L); 0.5 µm (K).

Journal of Cell Science (2018) 131, jcs212324. doi:10.1242/jcs.212324

(Fig. 4A-J). In wild-type MEFs, both GFP fusion proteins were distributed uniformly along the full length of cilia, overlapping with the distribution of the endogenous ARL13B protein (Fig. 4A-C). In contrast, in *Arl13b*^{hnn} MEFs, GFP-mARL13BΔGD localized to the very distal tip of the cilium and accumulated in expansions of the ciliary membrane, but it was undetectable or barely visible along the rest of the ciliary length (Fig. 4E). Occasionally, in shorter cilia, we also observed accumulation of GFP-mARL13BΔGD at the ciliary base but the GFP signal remained very low along the central region of the cilium (Fig. 4F). Finally, GFP-mARL13BΔGD concentrated in stump-like cilia of *Arl13b*^{hnn} MEFs (Fig. 4G). Cilia of variable length were also observed in non-transduced MEFs, as shown by staining with an antibody against acetylated tubulin (Fig. 4H-J). Ultrastructural analysis by transmission electron microscopy (TEM) of clonal mutant GFP-mARL13BΔGD-expressing *Arl13b*^{hnn} MEFs revealed that electron-dense material accumulated within the ciliary matrix – the space encompassed by the axoneme and the ciliary membrane – of the entire ciliary length and in stump-like cilia (Fig. 4K). This accumulation was not observed in the ciliary matrix of clonal *Arl13b*^{hnn} MEFs expressing the wild-type GFP-mARL13B (Fig. 4K). Interestingly, the distribution of electron-dense material observed along the entire cilium of *Arl13b*^{hnn} MEFs did not parallel the distribution of the membrane-associated GFP-mARL13BΔGD observed by immunofluorescence at the distal or proximal tip in the *Arl13b*^{hnn} MEFs cilia (Fig. 4E,F,L). These observations suggested that, in addition to its role in cilia assembly, the G-domain of ARL13B plays a role in the distribution of membrane proteins along the ciliary membrane.

To test this hypothesis, we analyzed membrane protein distribution along the cilium of ARL13B variants predicted or shown to interfere with the GTP-GDP exchange activity of ARL13B, including variant GFP-mARL13B T35N and variant GFP-mARL13B R79Q, which carries the Joubert-syndrome-causing mutation R79Q. In wild-type MEFs, wild-type and all mutant GFP fusion proteins tested distributed evenly along the cilium (Figs 3D and 4M). In contrast, in *Arl13b*^{hnn} MEFs, although GFP-ARL13B-ΔGD distribution was visibly affected in >80% of cilia, both GFP-mARL13B T35N and GFP-mARL13B R79Q distributed evenly along the cilium (Fig. 4L,M). Thus, the even distribution of ARL13B along the cilium depends on ARL13B interactions that occur within the G-domain but are independent of its GTPase activity.

To determine whether the localization of other ciliary membrane proteins was affected by the absence of ARL13B, we analyzed the distribution of SMO and somatostatin receptor 3 SSTR3 along the cilium of *Arl13b*^{hnn} and wild-type MEFs (Fig. 5). Consistent with previous studies, we found SMO evenly distributed along the cilium of SHH-stimulated wild-type MEFs and at slightly higher concentration at the ciliary base (Fig. 5A). Similarly, the ectopically expressed mCherry-tagged SSTR3 fusion protein (mCherry-SSTR3) also displayed uniform distribution along all the length of the ciliary membrane of wild-type MEFs (Fig. 5G). In contrast, in *Arl13b*^{hnn} MEFs SMO concentrated in discrete regions of the cilium located mostly at distal and/or proximal extremities of cilia regardless the presence of SHH in the medium (Fig. 5B). However, we noticed that SMO in cilia of SHH-stimulated *Arl13b*^{hnn} MEFs was almost exclusively detected at the distal tip of the cilium (Fig. 5B,E). Similarly, the mCherry-SSTR3 also failed to distribute evenly along the cilium and accumulated at the distal tip of *Arl13b*^{hnn} MEFs cilia (Fig. 5H). These results are consistent with previously reported observations (Larkins et al., 2011). Importantly, the aberrant distribution of SMO and mCherry-SSTR3 along the ciliary membrane in *Arl13b*^{hnn} MEFs could be rescued by wild-type GFP-ARL13B and by the GDP-locked variant ARL13 T35N, but not by GFP-mARL13BΔGD (Fig. 5C-F,I-L,M). These results indicate that ARL13B, independently of its GTPase activity, plays an important role in locating and maintaining the distribution of membrane proteins along the ciliary membrane.

ARL13B interacts with the axoneme through its tubulin-binding domain

To explain how membrane-associated ARL13B distributed evenly along the cilium length we hypothesized that the capacity of ARL13B binding to tubulin provides the means for the physical interaction with microtubules and, thus, retention along the axoneme. To test whether the G-domain of ARL13B is required to anchor ARL13B to the ciliary axoneme, we performed *in vitro* pull-down of GST-ARL13B fragments by using demembranated axonemes purified from isolated *Chlamydomonas* flagella (Alper et al., 2013). The assay showed that both full-length ARL13B and its G-domain can bind isolated axonemes, whereas the coil-coil domain of ARL13B does not (Fig. 6A). Moreover, deletion of the G-domain drastically decreased the ability of ARL13B to bind to axonemes (Fig. 6B).

To confirm the binding of ARL13B to the ciliary axoneme *in vivo*, we exposed distinct clones of ciliated wild-type MEFs that stably express comparable amounts of GFP-ARL13B or GFP-ARL13B-ΔGD (Fig. S5A) to different concentrations of Triton X-100 ranging from 0% to 0.05% prior to fixation; we then analyzed the retention of the GFP-fused proteins along the cilium. In absence of detergent, GFP signal was evenly distributed along the full length of all cilia of MEFs clones expressing either GFP-ARL13B or GFP-ARL13B-ΔGD. In contrast, after treatment with 0.025% Triton X-100 the GFP signal was undetectable along cilia of MEF expressing GFP-ARL13B-ΔGD while it remained visible on >50% of wild-type MEFs expressing GFP-ARL13B (Fig. 6C,D and Fig. S5B). Finally, 0.05% Triton X-100 removed both GFP constructs from the majority of MEFs (Fig. 6D). Similar experiments conducted on *Arl13b*^{hnn} MEFs expressing wild-type or mutant versions of GFP-ARL13B corroborated the importance of the G-domain regarding the interaction of ARL13B with the axoneme. Upon treatment with 0.1% Triton X-100 prior to fixation, the immunofluorescence signal was lost in the cilia of *Arl13b*^{hnn} MEFs expressing GFP-ARL13B-ΔGD but not completely lost in those expressing the GFP-ARL13B or GFP-ARL13BT35N (Fig. S5C). Taken together, *in vitro* as well as *in vivo* evidence revealed that ARL13B binds to the ciliary axoneme through residues located within the G-domain.

DISCUSSION

In this study, we have uncovered a functional interaction between the ARL13B – that, when carrying certain mutations causes Joubert syndrome – and tubulin. We demonstrate that this interaction is direct, occurs within the G-domain of ARL13B and is independent from the predicted ARL13B GTPase activity required for ciliary assembly. We also provide evidence that the ARL13B-tubulin interaction is required for uniform distribution of ARL13B and other membrane proteins along the ciliary membrane. Hence, we propose that ARL13B plays a key role in mediating interactions between ciliary membrane components and the axoneme.

GTPases and tubulin-binding domains

Our TAP approach led to the identification of tubulin as one of the main interactors of ARL13B. Because tubulin is one of the most abundant proteins in cells, we have carefully analyzed the

Journal of Cell Science (2018) 131, jcs212324. doi:10.1242/jcs.212324

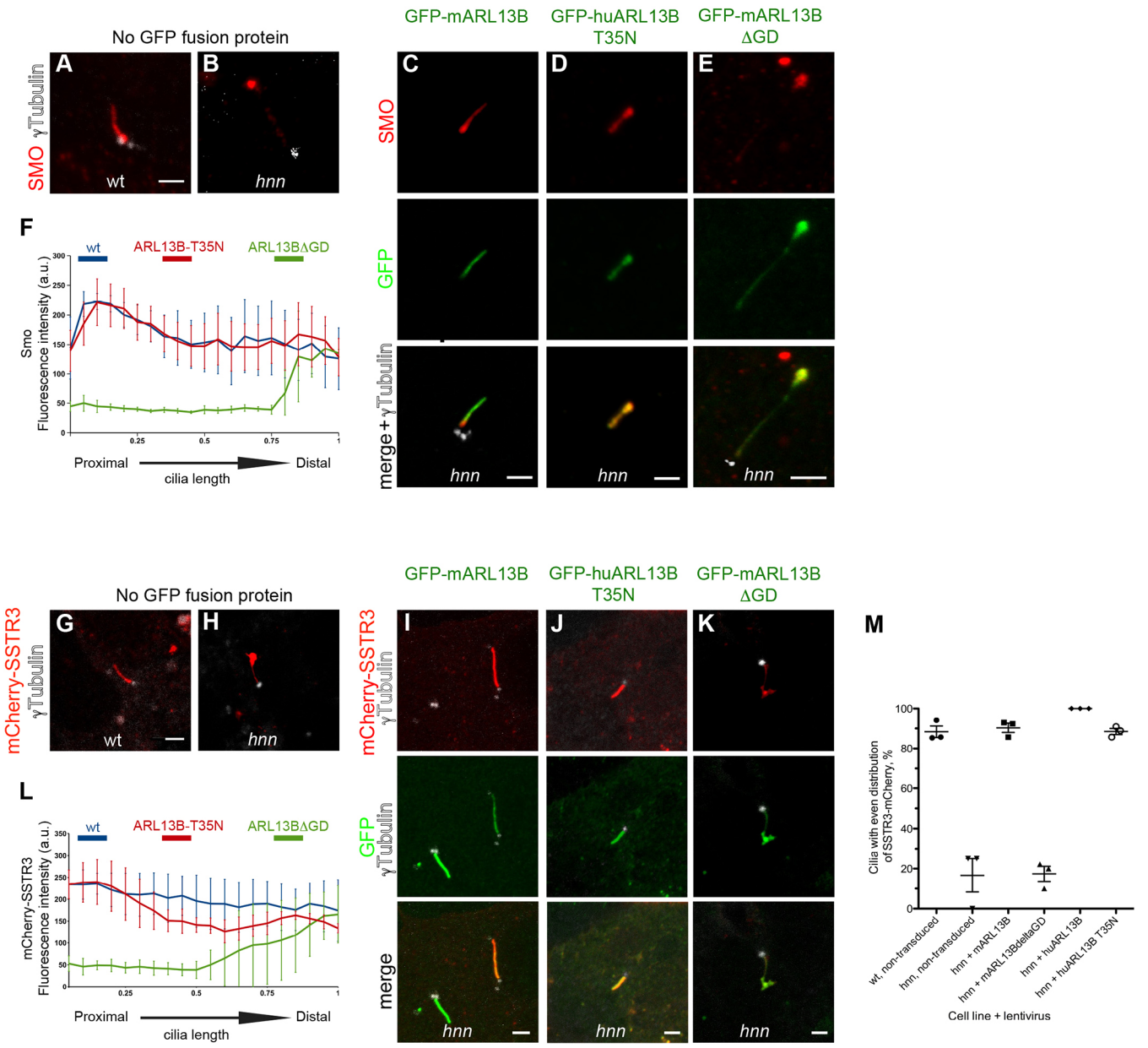

Fig. 5. The ARL13B G-domain sequence but not its GTPase activity is required for normal distribution of transmembrane proteins along the ciliary membrane. (A-E) Immunofluorescence signal for SMO (red), GFP (green) and γ-tubulin (white) in wild-type and *Arl13b*^{hnn} MEFs untransduced (A and B) and *Arl13b*^{hnn} MEFs stably expressing GFP-tagged wild-type or mutant ARL13B (C-E). MEFs shown in (A-E) were treated with recombinant SHH. (F) Average of fluorescence intensity (arbitrary units)±standard deviation of Smo along cilium length. *n*=20 cilia were evaluated for each construct and pooled from three independent experiments. Only cilia longer than 2 µm were analyzed. Student's *t*-test analysis of the differences between Smo signal intensity from MEFs expressing wild-type and mutant ARL13B, the error bar represents the s.d. For ARL13B-ΔGD, $P<0.0001$ for the proximal 80% of the cilia. For ARL13B-T35N, not significant along the entire length of the cilium. (G-K) Immunofluorescence signal for mCherry (red), GFP (green) and γ-tubulin (white) in wild-type and *Arl13b*^{hnn} MEFs transduced with mCherry-SSTR3 lentivector (G-K) and in *Arl13b*^{hnn} MEFs stably expressing GFP-tagged wild-type or mutant ARL13B (I-K). (L) Average of fluorescence intensity of mCherry-SSTR3 as calculated in (F). Student's *t*-test analysis of the differences between mCherry-SSTR3 signal intensity from MEFs expressing wild-type and mutant ARL13B, the error bars represent the mean ±s.d. For ARL13B-ΔGD, $P<0.001$ for the proximal 60% of the cilia. For ARL13B-T35N, not significant along the entire length of the cilium. (M) Quantification of cilia with even distribution of mCherry-SSTR3 (in %). The distribution was considered uneven when the fluorescence signal in any region of the cilium decreased >50% as compared to the signal intensity of the remaining portion of the cilium. Dots show the results of three independent experiments, error bars show means ±s.d. Cell lines and GFP-tagged ARL13b constructs are indicated below the graph. Scale bars: 2 µm.

specificity of this interaction using multiple approaches, including immunoprecipitation of native ARL13B from different cell lines and *in vitro* binding assays of purified tubulin or whole-cell extracts. Consistent with our finding, a proteomic approach using stable isotope labeling and affinity chromatography, identified 424 ARL13B-associated proteins, including several tubulin isotypes (Cevik et al., 2013). Tubulin isotypes including TUBB, TUBB6, TUBA4A, TUBB4B and TUBB3 were found in both the Cevik et al (2013) study and the present study. Small discrepancies between these two studies could be due to differences in sensitivity of the analytic approaches or the use of different cell lines. Pull-down experiments using GST fused to fragments of ARL13B allowed us

Journal of Cell Science (2018) 131, jcs212324. doi:10.1242/jcs.212324

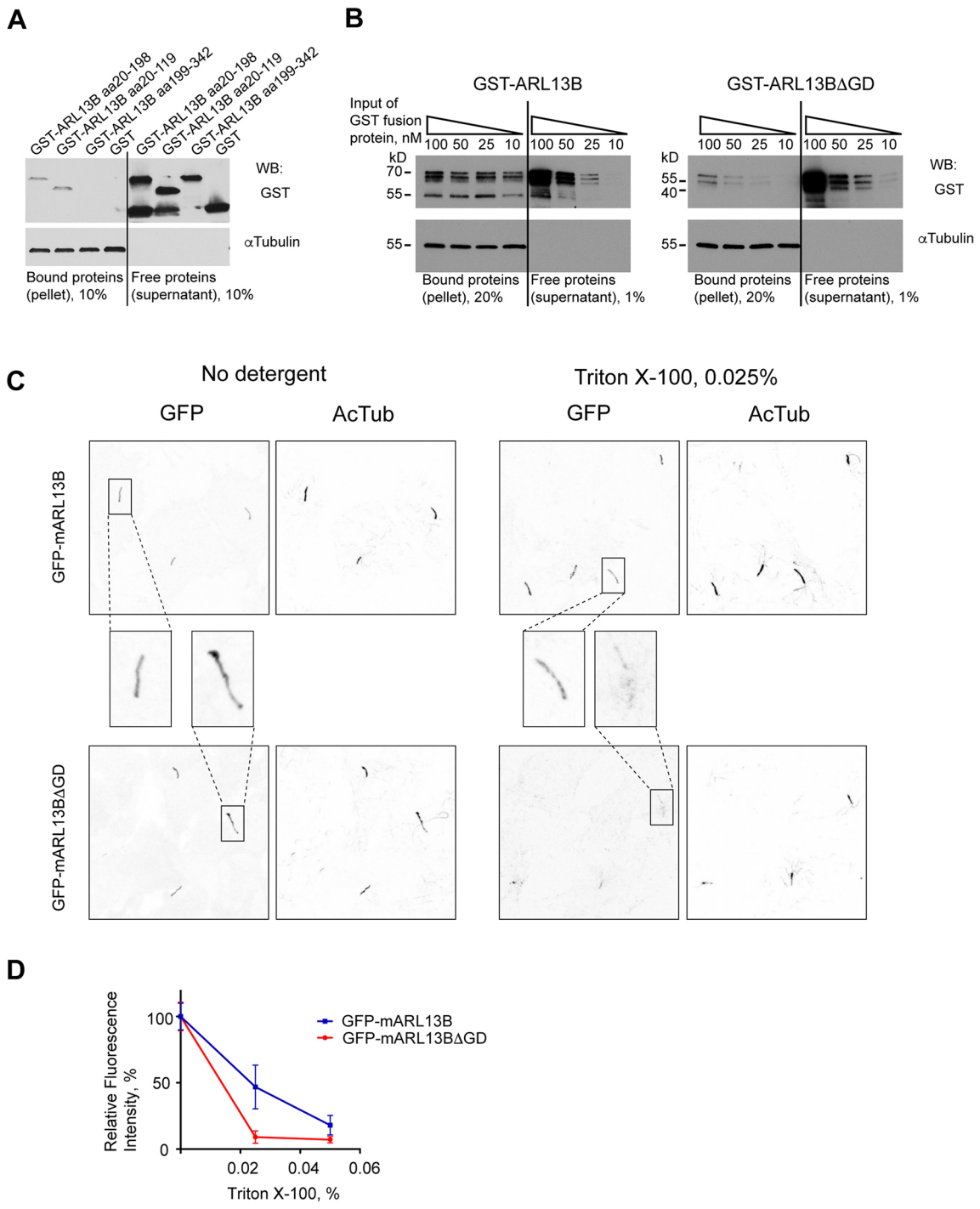

Fig. 6. Deletion of the G-domain weakens interaction of ARL13B with axonemes and association with cilia. (A,B) Arl13b G-domain is required for strong interaction with tubulin. (A) Purified fragments of ARL13B containing the G-domain co-sediment with isolated axonemes. Purified axonemes were incubated with solutions of GST fusion proteins and sedimented by centrifugation. Pellets and supernatants were analyzed by western blot. Only fragments containing the G-domain sequence bind to axonemes. (B) Progressively decreasing amounts of GST-ARL13B and GST-ARL13BΔGD independently incubated with equal amount of demembranated axoneme, sedimented by centrifugation and processed for WB (left lanes). Supernatant fractions containing free GST-tagged proteins not bound to the axonemes analyzed by WB (right lanes). Note that the amount of GST-ARL13B bound to the axoneme remains constant despite the drop of concentration of the GST-tagged protein loaded in the assay. In contrast, GST-ARL13BΔGD loses the interaction with the axoneme as the GST-tagged protein concentration decreases. (C) Confocal immunofluorescence of cilia of clonal wild-type MEFs stably expressing similar levels of GFP-ARL13B (upper panels, cell line 8A11) or GFP-ARL13BΔGD (lower panels, cell line 7A11) treated with PBS (control) or low concentrations of Triton X-100 in PBS. See also Fig. S6A for comparison of levels of expression of transgenes in MEFs. Single channels for GFP (ARL13B fusion proteins) and acetylated tubulin (axoneme) are shown in monochrome images. Wider microscope fields of images shown in right panels of C are shown in color in Fig. S5. (D) Quantification of GFP fusion proteins localized to cilia. Cilium areas were defined based on acetylated tubulin immunofluorescence signal. Original 12-bit images were used for quantifications of mean GFP immunofluorescence intensity ±s.d. Values were normalized to signals from non-treated cilia. Total number of quantified cilia per clone per each Triton X-100 concentration in two independent experiments were 17–26. GFP-ARL13B and GFP-ARL13BΔGD showed significant difference in Triton-dependent ciliary attachment (two-way ANOVA, P=0.0277).

Journal of Cell Science (2018) 131, jcs212324. doi:10.1242/jcs.212324

to map the tubulin-binding region within its G-domain. Despite this physical overlap, our data indicate that nucleotide binding does not modify the status of the ARL13B-tubulin interaction. In support of this conclusion, we found that the amount of tubulin interacting with ARL13B *in vitro* remains unchanged regardless the presence of GDP or the non-hydrolysable analog GTPγS. Moreover, point mutations in the ARL13B G-domain that reduce binding between ARL13B and GTP (R79Q) or abolish the predicted GTPase activity of ARL13B (T35N) did not alter binding between ARL13B and soluble tubulin or ARL13B and polymeric tubulin-based structures, including microtubules and demembranated axonemes. Human ARL13B T35N mutant exogenously expressed in *Arl13b*^{hnn} MEFs or used in tubulin-binding assays allowed us to uncouple GTPase activity from the interaction of ARL13B with tubulin. Our results indicate that the interaction between tubulin and ARL13B is pivotal to maintain a normal distribution of proteins along the ciliary membrane but it is not sufficient to rescue defects of cilia assembly and protein localization detected in absence of the wild-type ARL13B. Recent studies have shown that ARL13B is active as a GEF for ARL3 (Gotthardt et al., 2015; Zhang et al., 2016). Moreover, the T35N mutation in ARL13B and those that cause Joubert syndrome nearly abolish or reduce this activity, respectively (Ivanova et al., 2017). Thus, binding between ARL13B and tubulin appears dispensable for ARL13B GEF activity on ARL3. Interestingly, other members of the Arl family, including ARL7 and ARL8 were found to interact with tubulin and interfere with microtubule-driven cellular processes, such as intracellular vesicular transport and chromosome segregation, respectively (Okai et al., 2004; Wei et al., 2009). Moreover, ARL2 binds to the tubulin cofactor D and, together with ARL3, modulates microtubules dynamics and polymerization (Bhamidipati et al., 2000; Zhou et al., 2006). Although mammalian ARL6, a protein that can cause Bardet-Biedl syndrome when mutated (also known as BBS3), does not contain the amphipathic N-terminal domain, its *Trypanosoma brucei* orthologue interacts with the ciliary membrane and with tubulin (Price et al., 2012). Intriguingly, ultrastructural analysis revealed an evolutionarily conserved role of ARL13B in maintaining the structural integrity of the cilium. The ARL13B-null mutation Arl13b$^{hnn/hnn}$ in mouse and deletion of aa 169–342 within the Arl13b protein in *C. elegans*, lead to an open B-tubule of the axonemal doublets, further supporting a role for ARL13B on axonemal microtubules integrity (Caspary et al., 2007; Cevik et al., 2010).

However, because ARL13B is also required for cilia localization of other components of the ciliary membrane, such as INPP5E, it cannot be excluded that these axoneme-related structural defects are an indirect consequence of ARL13B dysfunction in protein translocation into the ciliary compartment. Moreover, consistent with previous studies, levels of acetylated and glutamylated axonemal tubulin, as revealed by immunolabeling, appear lower in cells lacking ARL13B compared to control cells (Larkins et al., 2011; Nozaki et al., 2017). However, we found that absence or presence of wild-type or mutant ARL13B variants had no effect on the overall cellular levels of acetylated or polyglutamylated tubulin (Fig. S6). Thus, whether ARL13B has an effect on tubulin polymerization/depolymerization, on levels of post-translational modified tubulin in the axoneme or in shaping axonemal architecture remains to be established.

The G-domain is dispensable for ciliary translocation of ARL13B to cilia

Although it has been shown that GFP-tagged N-terminal or C-terminal domains of ARL13B fail to localize to cilia it has also been demonstrated that ARL13B interactions with the membrane through palmitoylation or myristoylation at the N-terminus are critical for its compartmentalization (Cevik et al., 2010; Duldulao et al., 2009; Hori et al., 2008; Larkins et al., 2011; Zhou and Anderson, 2010). To preserve such interactions, we maintained the N-terminal amphipathic helix (aa 1–19) in all our constructs. In agreement with Nozaki et al., 2017, GFP-ARL13B-ΔGD maintained cilia localization although it was unable to rescue the defective cilia phenotype of *Arl13b*^{hnn} MEFs. Thus, these observations strongly suggest that the G-domain of ARL13B plays a crucial role in ciliary assembly and membrane protein distribution along the ciliary membrane, although it is dispensable for ARL13B trafficking to the ciliary compartment. These data confirm previous results for the T35N mutation and are in agreement with the findings that other point mutations that also affect the active site of ARL13B G-domain, i.e. R79Q and T38N, do not interfere with ARL13B trafficking to the cilium (Cantagrel et al., 2008; Cevik et al., 2013; Duldulao et al., 2009; Hori et al., 2008; Mariani et al., 2016; Miertzschke et al., 2014). Furthermore, our findings strongly suggest that the G-domain and its interaction with tubulin are dispensable for targeting ARL13B to cilia. However, it cannot be excluded that trafficking may be regulated by conformational changes in the G-domain, which might, in turn, affect, for example, exposure of the amphipathic helix, as shown for ARF1 (Levi et al., 2008).

ARL13B mediates interactions between the ciliary membrane and the axoneme to maintain uniform distribution of proteins along the ciliary membrane

We have shown that, although GFP-ARL13B-ΔGD can enter the cilium of *Arl13b*^{hnn} MEFs, it accumulates preferentially at the distal ciliary tip or – less frequently – at both proximal and distal ciliary extremities. Moreover, other ciliary membrane proteins including SMO and SSTR3 display a similar non-uniform distribution along the cilium of *Arl13b*^{hnn} MEFs. This is in striking contrast to the uniform ciliary distribution of GFP-ARL13B, which also rescues the short-cilia phenotype of the *Arl13b*^{hnn} MEFs. Importantly, we have shown that GFP-mARL13B T35N, which allowed us to uncouple the interaction between ARL13B and tubulin from the GTPase activity of ARL13B, can restore the uniform distribution of ARL13b, SMO and SSTR3 but not the short-cilia phenotype of *Arl13b*^{hnn} MEFs. Consistent with these findings, the ciliary protein GPR161, which negatively regulates Hh signaling, displays a non-uniform ciliary distribution (and mostly accumulated at the tip of the cilium) in ARL13B-deficient cells under basal and Hedgehog-stimulated conditions (Nozaki et al., 2017). The discrete localization and accumulation of GFP-ARL13B-ΔGD at the ciliary tip could be linked to defective localization of IFT components that in *Arl13b*^{hnn} MEFs accumulate mostly at the ciliary tip (Fig. S4) and (Nozaki et al., 2017). It was reported that ARL13B interacts with the IFT46–IFT56 heterodimer, components of the IFT complex B. Although this interaction is not necessary for ARL13B localization to cilia, it could be required to move ARL13B along the cilium during anterograde IFT. Consistent with this possibility, GFP-ARL13B-ΔGD maintains its interaction with IFT complex B (Nozaki et al., 2017). In addition, the lack of the G-domain has been suggested to interfer with the function of IFT complex A in retrograde movement and might further explain the accumulation of GFP-ARL13B-ΔGD at the ciliary tip and its depletion in other ciliary regions (Iomini et al., 2009; Mukhopadhyay et al., 2010; Nozaki et al., 2017). How can the ARL13B interaction with tubulin mediate protein distribution along

Journal of Cell Science (2018) 131, jcs212324. doi:10.1242/jcs.212324

the ciliary membrane? Based on our results we speculate that ARL13B plays a pivotal role in mediating interactions between the ciliary membrane and the axoneme. Interestingly, we found that GFP-ARL13B-ΔGD distributes uniformly along the cilium of wild-type MEFs. Thus, the presence of wild-type endogenous ARL13B allows correct localization of exogenous GFP-ARL13B-ΔGD. Nevertheless, *in vitro* and *in vivo* binding assays to the axoneme revealed that interaction of GFP-ARL13B-ΔGD with the axoneme is weakened, even in presence of the wild-type endogenous ARL13B. This could be due to the existence of ARL13B homophilic interactions with other ARL13B molecules along the axoneme. It has been shown that ARL13B can be simultaneously localized at the membrane or move together with IFT particles (Cevik et al., 2013). Another pool of ARL13B molecules could bind to the axoneme and, thus, anchor other ARL13B molecules by direct binding. In support of this possibility, it was shown that ARL13B self-associates, as shown by immunoprecipitation (Hori et al., 2008). In our model, a pool of ARL13B molecules binds to the axoneme via regions of the G-domain; however, other ARL13B molecules might form protein complexes connecting the ciliary membrane and the axoneme. Our data show the acetylation of α−tubulin molecules that interact with ARL13B – which supports this possibility – since axonemal tubulin is highly acetylated (Fig. 1). Elegant ultrastructural studies of cilia in different model systems have clearly documented the presence of a variety of electron-dense bridges that link the ciliary membrane with the axonemal microtubules along the length of the cilium and flagellum, as well as at the ciliary extremities reviewed by Dentler, 1990. Moreover, biochemical fractionation of *Chlamydomonas* flagella combined with proteomic analysis has revealed that, surprisingly, axonemal fractions of detergent-extracted flagella contain a large number of transmembrane proteins in addition to axonemal proteins (Pazour et al., 2005). This finding strongly supports the existence of interactions (direct or indirect) between ciliary membrane proteins and the axoneme. Our data suggest that ARL13B plays a critical role in mediating and/or regulating these interactions. Further studies, specifically tailored to uncover molecular components and mechanisms underlying axoneme-membrane interactions, will broaden our understanding of cilia-mediated signal transduction.

MATERIALS AND METHODS

Plasmids and lentiviral vectors

The TAP-tag plasmid vectors pIC112 and pIC113 (Cheeseman and Desai, 2005) were provided by Dr Iain Cheeseman, Whitehead Institute for Biomedical Research, Cambridge, MA. To express TAP-tagged ARL13B in mammalian cells, the sequence 5′-GATATCGGCCTAGGAAGGTACC AAGGATCCGGGAATTCAGAGCACGTGGGC-3′ containing various cloning sites was inserted between the NheI and NotI sites of the VVEW/BB lentivector (Battini et al., 2008) to generate VEB2. The NheI–SpeI fragment encoding the GFP-TEV-S tag was excised from pIC113 and inserted into the NheI site of VEB2 to generate VEB113. Alternatively, VEB2 was digested with PmlI and NotI and the ends were filled-in using *PfuUltra* DNA polymerase (Agilent Technologies, Santa Clara, CA). The EcoRV–PmeI fragment encoding the 6×His-PreScission-mRFP tag was excised from pIC112 and inserted into VEB2 to generate VEB112. To express GFP-TEV-S-tagged mouse ARL13B, wild-type mouse *Arl13b* cDNA (NCBI Reference Sequence: NM_026577.3) was amplified by PCR using PrimeSTAR HS DNA polymerase (Clontech), plasmid pMEmArl13bGFP as a template and primers Arl13/113/Kpn/5 (5′-GTGG-TACCAAATGTTCAGTCTGATGGCCAACTGCTGCAACTTG-3′) and Arl13/113/Bam/3 (5′-GTGGTACCAAATGTTCAGTCTGATGGCCAAC-TGCTGCAACTTG-3′).

Plasmids for expression of wild-type human ARL13B or mutant ARL13B carrying the R79Q substitution (pGEX-ARL13B and pGEX-ARL13B R79Q, respectively) (Cantagrel et al., 2008), were a gift from Dr Joseph Gleeson, UCSD, La Jolla, CA. To express human GFP-TEV-S-tagged ARL13B, cDNA was amplified by PCR using pGEX-ARL13B or pGEX-ARL13B R79Q and primers ARL13BHu-113-Kpn5 (5′-GTGGT-ACCAAATGTTCAGTCTGATGGCCAGTTGC-3′) and ARL13BHu-113-Bam3 (5′-GAGGATCCTATTATGAGATCACATCATGAGCATCACTG-TTAG-3′). The PCR fragments were digested with restriction endonucleases KpnI and BamHI, and inserted between the KpnI and BamHI sites of VEB113 to generate VEB113-GFP-TEV-S-mArl13b, VEB113-GFP-TEV-S-huARL13B or VEB113-GFP-TEV-S-huARL13B-R79Q. To express GFP-TEV-S-tagged mouse ARL13B lacking the coiled-coil domain or the G-domain, the corresponding cDNA fragments were joined by PCR and inserted into VEB113-GFP-TEV-S-mArl13b between the AvrII and BamHI sites, or between the AvrII and BstXI sites. Plasmid for expression of human ARL13B with the point mutation T35N (pSSN-huARL13B T35N) (Humbert et al., 2012) was a gift from Dr Seongjin Seo, University of Iowa, Iowa City, IA. To express GFP-TEV-S-tagged human ARL13B with the point mutations, cDNAs were amplified by PCR and inserted between the KpnI and BamHI sites of VEB113.

To express 6XHis-PreScission-mRFP-tagged mouse ARL13B, wild-type mouse *Arl13b* cDNA (NCBI Reference Sequence: NM_026577.3) was amplified by PCR using the plasmid pME mARL13b GFP and primers Arl13/112/Kpn/5 (5′-gaggtaccgccatgttcagtctgatggccaactgctgcaacttgttc-3′) and Arl13/112/Bam/3 (5′-gaggatcctgagatcgtgtcctgagcatcaccgttaggtctctg-3′).

To express 6XHis-PreScission-mRFP-tagged human ARL13B, cDNA was amplified using pGEX-ARL13B or pGEX-ARL13B R79Q (Cantagrel et al., 2008) and primers ARL13BHu-112-Kpn-5 (5′-GAGGT-ACCGCCATGTTCAGTCTGATGGCCAGTTGC-3′) and ARL13BHu-112-Bam-3 (5′-GAGGATCCTGAGATCACATCATGAGCATCACTGT-TAG-3′). The fragments were digested with restriction endonucleases KpnI and BamHI and inserted between the KpnI and BamHI sites of VEB112 to generate VEB112-mArl13b-6xHis-PreScission-mRFP or VEB112-huARL13B-6xHis-PreScission-mRFP. All the constructs were confirmed by sequencing. Lentivirus-containing supernatants were produced by transient transfection of Lenti-X 293T cells (Clontech) as described previously (Fedorova et al., 2006).

Cell culture, transfection and lentivirus transduction, and activation of the Hh signaling

Immortalized human retinal pigment epithelium hTERT RPE-1 (ATCC® CRL-400™) were grown in high-glucose DMEM, 10% fetal bovine serum (FBS). Immortalized wild-type and *Arl13b*^{hnn} MEFs were a gift of Dr Tamara Caspary, Emory University, Atlanta, GA. For immunofluorescence, MEFs were grown on gelatinized glass coverslips in high-glucose DMEM, 10% FBS. Transfection with plasmid SSTR3-mCherry (Addgene) was performed using X-treme GENE 9 DNA transfection reagent (Roche Diagnostics) according to the manufacturer's instructions. For transduction, lentiviral particles were resuspended in serum-free DMEM and added to cells grown in high-glucose DMEM, 10% FBS. Medium was replaced after 24 h. Treatment with SHH was performed as described (Larkins et al., 2011) using human recombinant SHH (StemRD) at 5 ng/ml in high glucose DMEM, 0.5% FBS.

Tandem affinity purification, mass-spectrometry and database searching

A stable cell line of hTERT RPE-1 expressing GFP-TEV-Stag-ARL13B (VEB113) was generated by using a lentiviral expression vector as previously described (Nachury, 2008). Cells were selected by using blasticidin at 10 µg/ml and sorted by FACS. For TAP, cells from a selected clone or wild-type control were grown on 15-cm dishes to confluency and serum-starved for 48 h to induce ciliogenesis. Cell lysates were prepared from 1.5 ml of packed cell pellets and ARL13B-interacting proteins were purified as described (Nachury, 2008; Torres et al., 2009). Proteins were separated on a 4–15% polyacrylamide TGX gel (Bio-Rad), stained using the SilverQuest Silver Staining kit (Life Technologies) and analyzed by western blotting. For tandem MS, gels were stained using the Colloidal Blue staining kit (Life Technologies).

Individual bands were excised manually. Samples were prepared and processed at the Proteomics and Microchemistry Core facility (Memorial Sloan Kettering Cancer Center, New York, NY), as described previously (Schwer et al., 2011). All tandem MS samples were analyzed using Mascot (Matrix Science, London, UK; version 2.3.02) and X! Tandem (The GPM, thegpm.org; version CYCLONE 2010.12.01.1). Mascot was set up to search the Uniprot_sprot_20120815 database (selected for Homo sapiens, 20306 entries), assuming the digestion enzyme trypsin. X!Tandem was set up to search a subset of the uniprot_sprot_20120815 database and also assuming trypsin digestion. Mascot and X! Tandem were searched with a fragment ion mass tolerance of 0.80 Da and a parent ion tolerance of 10.0 ppm. Deamidation of Asx and Gln, oxidation of Met, acetylation of the N-terminus and propionamidation of Cys were specified in Mascot and X! Tandem as variable modifications.

Scaffold (version Scaffold_3.6.4, Proteome Software Inc., Portland, OR) was used to validate MS/MS-based peptide and protein identifications. Protein identifications were accepted when they could be established at >95.0% probability and contained ≥1 identified peptides. Protein probabilities were assigned by the PeptideProphet algorithm (Nesvizhskii et al., 2003).

Immunoprecipitation, protein expression and purification, GST pull-down assay

Cell extracts were prepared as described (Miserey-Lenkei et al., 2010). 500 µg of total cell protein in the extraction buffer supplemented with protease inhibitor cocktail cOmplete mini, EDTA-free (Roche Diagnostics), 10 mM $MgCl_2$ and 0.1% NP-40 (Igepal CA-630, Sigma) was incubated with 1 µg of polyclonal antibody (pAb) anti-ARL13B (Abcam, ab18251) or rabbit IgG (Bethyl) at 4°C for 16 h. 10 µl of Pierce protein A agarose beads (ThermoFisher) was added and the mixture was incubated for 2 h. Beads were washed five times with 25 mM Tris pH 7.5, 10 mM $MgCl_2$, 50 mM NaCl, 0.1% NP40, eluted with 2× Laemmli loading buffer at 95°C, and proteins were loaded onto 4–15% TGX gel (Bio-Rad). Proteins were detected by western blotting.

For expression of GST-tagged wild-type human ARL13B and ARL13B mutant protein carrying the mutation R79Q, plasmids pGEX-ARL13B and pGEX-ARL13B R79Q were used, respectively, (Cantagrel et al., 2008) were used. For analysis of truncated domains of ARL13B, fragments of its cDNA were amplified by PCR using PrimeSTAR HS DNA polymerase (Clontech) and inserted into pGEX-6P-1 (GE Healthcare) between the BamHI and NotI sites. To express GST-huARL13B T35N the cDNA was amplified using pSSN-huARL13B T35N (Humbert et al., 2012). To express human ARL13B lacking the G-domain, the cDNA fragments flanking the deletion were joined by PCR and the resulting fragment was inserted into pGEX-ARL13B between the BamHI and SpeI sites. Control GST protein was expressed using pGEX-4T-2 (GE Healthcare). All constructs were confirmed by sequencing. GST-tagged wild-type human ARL13B and its mutated variants were expressed in *Escherichia coli* strain BL21 – CodonPlus (DE3)-RIL (Agilent Technologies). Protein purification was performed as described previously (Hori et al., 2008). To remove glutathione, eluted proteins were dialyzed against Buffer A [50 mM Tris-HCl, pH 7.5, 100 mM NaCl, 5 mM $MgCl_2$, 1 mM DTT, 0.1% (w/v) Triton X-100, protease inhibitor cocktail complete mini, EDTA-free (Roche Diagnostics)] according to Hori et al., 2008 using Slide-A-Lyzer dialysis cassettes with a molecular mass cut-off at 10 kDa (Thermo Scientific).

For GST pull-down assay 20 µl of Glutathione Sepharose 4B beads (GE Healthcare) was equilibrated with Buffer A according to Hori et al., 2008, and incubated with 20 pmoles of GST fusion protein in 200 µl Buffer A, 1 mM DTT, 0.1% Triton X-100, for 2 h at 4°C with rotation. Beads were washed and incubated in Buffer A supplemented with 200 µM of GTPγS or GDP and 5 mM EDTA for 1 h at room temperature (24°C). Buffer A was replaced with cell extract containing 100 µg of total protein in LAP100 buffer supplemented with protease inhibitor cocktail cOmplete mini, EDTA-free (Roche Diagnostics), 200 µM of GTPγS or GDP (Sigma), 10 mM $MgCl_2$, and 0.3% (w/v) NP-40 (Igepal CA-630, Sigma, I3021). In the assays that tested binding to purified tubulin, 100 pmoles of bovine tubulin (>99% pure, Cytoskeleton, Cat. # T240) in 100 µl of LAP100 buffer supplemented with 1 mg/ml of bovine serum albumin (BSA; New England Biolabs), protease inhibitor cocktail cOmplete mini, EDTA-free, 200 µM of GTPγS or GDP, 10 mM $MgCl_2$, and 0.3% (w/v) NP-40 (Igepal CA-630, Sigma, I3021). Beads were incubated under rotation at room temperature for 90 min, washed four times with Buffer A supplemented with 10 mM $MgCl_2$, 0.1% Triton X-100, and bound proteins were eluted with 2× Laemmli loading buffer at 95°C.

Immunostaining and transmission electron microscopy

Cells were seeded on coverslips and grown in high-glucose DMEM supplemented with 10% FBS. To induce ciliogenesis, medium was replaced with serum-free high-glucose DMEM for 24–48 h. To induce accumulation of SMO in the ciliary compartment, cells were treated with 5 ng/ml recombinant Sonic Hedgehog (StemRD, Burlingame, CA) during the last 14–16 h of treatment with serum-free DMEM. For electron microscopy, cells were fixed in 2.5% glutaraldehyde in 0.1 M sodium cacodylate buffer for 16 h at 4°C. Transmission electron microscopy (TEM) was carried out as described (Grisanti et al., 2016). For immunostaining, cells were fixed with 4% PFA in PBS at 4°C or cold methanol for 10–15 min and permeabilized with 0.1% Triton X-100 in PBS for 10 min at room temperature. After blocking for 1 h with 2% BSA in PBS the primary antibodies diluted in 2% BSA in PBS were applied for 2 h. Secondary antibodies diluted in PBS were applied for 1 h after 3 washes of 10 min. Coverslips were mounted in Vectashield with or without DAPI (Vector Laboratories, Burlingame, CA) and analyzed using a Zeiss LSM510 and LSM880 confocal microscopes. Confocal images were captured with Plan-Neofluar 40×/1.3 Oil and a Plan-Apochromat 63×/1.4 Oil objectives and the acquisition software ZEN Black (Zeiss). The images were exported, analyzed with ImageJ and processed in Photoshop 7.0.1 and Illustrator CS6 (Adobe Systems). Levels of fluorescence intensity of GFP-tagged ARL13B constructs were measured using line-scan-based analysis in ImageJ. The average intensity over a three-pixel-wide line along the axoneme was measured and plotted against normalized cilium length.

The following primary antibodies were used: rabbit anti-α-tubulin pAb (Abcam, ab18251), mouse anti-β-tubulin monoclonal antibody (mAb) (Sigma, T4026), goat anti-γ-tubulin pAb (Santa Cruz Biotechnology, sc-7396), mouse anti-acetylated tubulin mAb (Sigma, T7451), mouse anti-polyglutamylated tubulin mAb (Enzo Life Sciences, ALX-804-885), mouse anti-ARL13B mAb (UC Davis/NIH NeuroMab Facility, clone N295B/66), rabbit anti-ARL13B pAb (Proteintech, 17711-1-AP), mouse anti-GFP mAb (Life Technologies, A11120), rabbit anti-GFP pAb (Life Technologies, A11122), mouse anti-GST mAb (GenScript, A00865), rabbit anti-S-tag pAb (GenScript, A00625), rabbit anti-IFT88 pAb (Proteintech, 13967-1-AP), mouse anti-dykddddk (anti-FLAG) mAb (Sigma, F3165), mouse anti-actin mAb (EMD Millipore, MAB1501), rabbit anti-SMO pAb (1:500) was a gift of Dr Kathryn V. Anderson, Memorial Sloan Kettering Cancer Center, New York, NY. Secondary antibodies used for immunofluorescence were FITC-conjugated AffiniPure donkey anti-mouse or anti-rabbit IgG (Jackson Immunoresearch, 715-095-150 or 711-095-152, respectively), TRITC-conjugated AffiniPure donkey anti-mouse or anti-rabbit IgG (Jackson Immunoresearch, 715-025-150 or 711-025-152, respectively), Alexa Fluor 555 donkey anti-rabbit IgG (Life Technologies, A31572), Alexa Fluor 647 donkey anti-goat (Life Technologies, A21447). Secondary antibodies used for western blotting were HRP-conjugated goat anti-mouse or anti-rabbit IgG (1:500–1:1000; Pierce; 1858413, 1858415, respectively). Antibodies were diluted as suggested by vendor recommendation when not specified.

Axoneme isolation and binding assays

Chlamydomonas reinhardtii wild-type cells were cultured and flagella isolated as previously described (Iomini et al., 2001). Axonemes were demembranated and isolated as described by Alper et al., 2013. Demembranated axonemes were resuspended in 200 µl of HMDEKP buffer [30 mM HEPES, pH 7.4, 5 mM $MgSO_4$, 1 mM DTT, 1 mM EGTA, 50 mM K-acetate, 1% (w/v) PEG] with proteinase inhibitor cocktail cOmplete mini, EDTA-free (Roche Diagnostics). For binding assays, 20 µl of the axoneme suspension was mixed with 2–20 pmoles of GST fusion protein in 200 µl Buffer A (Hori et al., 2008), 1 mM DTT, 0.1% triton X-100, and incubated for 2 h at room temperature with rotation. Axonemes were precipitated by centrifugation at 15,996 ***g*** for 10 min, washed five times in Buffer A, and dissolved together with bound proteins in 2× Laemmli loading buffer at 95°C.

Acknowledgements
We thank Iain Cheeseman for providing the TAP-tag plasmid vectors pIC112 and pIC113. Plasmids for protein expression were a gift from Joseph Gleeson, Tamara Caspary and Seongjn Seo. Antibody anti-SMO was kindly provided by Kathryn V. Anderson. We are grateful to Yaseris Rosario-Peralta and Ron Gordon for help with ultrastructural analysis and all Mlodzik and Iomini lab members for very helpful input and discussion. Confocal microscopy and cell sorting were performed at the Microscopy and the Flow Cytometry CoREs at the Icahn School of Medicine at Mount Sinai, respectively.

Competing interests
The authors declare no competing or financial interests.

Author contributions
Conceptualization: E.R., G.L.G., C.I.; Methodology: E.R., G.L.G., C.I.; Validation: E.R., C.I.; Formal analysis: E.R., Q.L., C.I.; Investigation: E.R., Q.L., G.L.G., C.I.; Resources: G.L.G., C.I.; Data curation: E.R., C.I.; Writing - original draft: E.R., C.I.; Writing - review & editing: E.R., G.L.G., C.I.; Visualization: E.R., C.I.; Supervision: C.I.; Project administration: C.I.; Funding acquisition: G.L.G., C.I.

Funding
This work was supported by National Institutes of Health grants R01DK106035 to G.L.G. and R01EY022639 to C.I. and the Research to Prevent Blindness Dolly Green Special Scholar Award to C.I. Deposited in PMC for release after 12 months.

Supplementary information
Supplementary information available online at
http://jcs.biologists.org/lookup/doi/10.1242/jcs.212324.supplemental

References

Alper, J., Geyer, V., Mukundan, V. and Howard, J. (2013). Reconstitution of flagellar sliding. *Methods Enzymol.* **524**, 343-369.
Barral, D. C., Garg, S., Casalou, C., Watts, G. F. M., Sandoval, J. L., Ramalho, J. S., Hsu, V. W. and Brenner, M. B. (2012). Arl13b regulates endocytic recycling traffic. *Proc. Natl. Acad. Sci. USA* **109**, 21354-21359.
Battini, L., Macip, S., Fedorova, E., Dikman, S., Somlo, S., Montagna, C. and Gusella, G. L. (2008). Loss of polycystin-1 causes centrosome amplification and genomic instability. *Hum. Mol. Genet.* **17**, 2819-2833.
Bhamidipati, A., Lewis, S. A. and Cowan, N. J. (2000). ADP ribosylation factor-like protein 2 (Arl2) regulates the interaction of tubulin-folding cofactor D with native tubulin. *J. Cell Biol.* **149**, 1087-1096.
Cantagrel, V., Silhavy, J. L., Bielas, S. L., Swistun, D., Marsh, S. E., Bertrand, J. Y., Audollent, S., Attié-Bitach, T., Holden, K. R., Dobyns, W. B. et al. (2008). Mutations in the cilia gene ARL13B lead to the classical form of Joubert syndrome. *Am. J. Hum. Genet.* **83**, 170-179.
Casalou, C., Seixas, C., Portelinha, A., Pintado, P., Barros, M., Ramalho, J. S., Lopes, S. S. and Barral, D. C. (2014). Arl13b and the non-muscle myosin heavy chain IIA are required for circular dorsal ruffle formation and cell migration. *J. Cell Sci.* **127**, 2709-2722.
Caspary, T., Larkins, C. E. and Anderson, K. V. (2007). The graded response to Sonic Hedgehog depends on cilia architecture. *Dev. Cell* **12**, 767-778.
Cevik, S., Hori, Y., Kaplan, O. I., Kida, K., Toivenon, T., Foley-Fisher, C., Cottell, D., Katada, T., Kontani, K. and Blacque, O. E. (2010). Joubert syndrome Arl13b functions at ciliary membranes and stabilizes protein transport in Caenorhabditis elegans. *J. Cell Biol.* **188**, 953-969.
Cevik, S., Sanders, A. A. W. M., Van Wijk, E., Boldt, K., Clarke, L., van Reeuwijk, J., Hori, Y., Horn, N., Hetterschijt, L., Wdowicz, A. et al. (2013). Active transport and diffusion barriers restrict Joubert Syndrome-associated ARL13B/ARL-13 to an Inv-like ciliary membrane subdomain. *PLoS Genet.* **9**, e1003977.
Cheeseman, I. M. and Desai, A. (2005). A combined approach for the localization and tandem affinity purification of protein complexes from metazoans. *Sci. STKE* **2005**, pl1.
Cool, R. H., Schmidt, G., Lenzen, C. U., Prinz, H., Vogt, D. and Wittinghofer, A. (1999). The Ras mutant D119N is both dominant negative and activated. *Mol. Cell. Biol.* **19**, 6297-6305.
Dascher, C. and Balch, W. E. (1994). Dominant inhibitory mutants of ARF1 block endoplasmic reticulum to Golgi transport and trigger disassembly of the Golgi apparatus. *J. Biol. Chem.* **269**, 1437-1448.
Dentler, W. L. (1990). Linkages between microtubules and membranes in cilia and flagella. In *Ciliary and Flagellar Membranes* (ed. R. A. Bloodgood), pp. 31-64. New York: Plenum Press.
Deretic, D., Williams, A. H., Ransom, N., Morel, V., Hargrave, P. A. and Arendt, A. (2005). Rhodopsin C terminus, the site of mutations causing retinal disease, regulates trafficking by binding to ADP-ribosylation factor 4 (ARF4). *Proc. Natl. Acad. Sci. USA* **102**, 3301-3306.
Donaldson, J. G. and Jackson, C. L. (2011). ARF family G proteins and their regulators: roles in membrane transport, development and disease. *Nat. Rev. Mol. Cell Biol.* **12**, 362-375.
Dorn, K. V., Hughes, C. E. and Rohatgi, R. (2012). A Smoothened-Evc2 complex transduces the Hedgehog signal at primary cilia. *Dev. Cell* **23**, 823-835.
Duldulao, N. A., Lee, S. and Sun, Z. (2009). Cilia localization is essential for in vivo functions of the Joubert syndrome protein Arl13b/Scorpion. *Development* **136**, 4033-4042.
Emmer, B. T., Maric, D. and Engman, D. M. (2010). Molecular mechanisms of protein and lipid targeting to ciliary membranes. *J. Cell Sci.* **123**, 529-536.
Fedorova, E., Battini, L., Prakash-Cheng, A., Marras, D. and Gusella, G. L. (2006). Lentiviral gene delivery to CNS by spinal intrathecal administration to neonatal mice. *J. Gene Med.* **8**, 414-424.
Feig, L. A. (1999). Tools of the trade: use of dominant-inhibitory mutants of Ras-family GTPases. *Nat. Cell Biol.* **1**, E25-E27.
Fujiu, K., Nakayama, Y., Yanagisawa, A., Sokabe, M. and Yoshimura, K. (2009). Chlamydomonas CAV2 encodes a voltage- dependent calcium channel required for the flagellar waveform conversion. *Curr. Biol.* **19**, 133-139.
Geng, L., Okuhara, D., Yu, Z., Tian, X., Cai, Y., Shibazaki, S. and Somlo, S. (2006). Polycystin-2 traffics to cilia independently of polycystin-1 by using an N-terminal RVxP motif. *J. Cell Sci.* **119**, 1383-1395.
Gotthardt, K., Lokaj, M., Koerner, C., Falk, N., Giessl, A. and Wittinghofer, A. (2015). A G-protein activation cascade from Arl13B to Arl3 and implications for ciliary targeting of lipidated proteins. *Elife* **4**.
Grisanti, L., Revenkova, E., Gordon, R. E. and Iomini, C. (2016). Primary cilia maintain corneal epithelial homeostasis by regulation of the Notch signaling pathway. *Development* **143**, 2160-2171.
Hori, Y., Kobayashi, T., Kikko, Y., Kontani, K. and Katada, T. (2008). Domain architecture of the atypical Arf-family GTPase Arl13b involved in cilia formation. *Biochem. Biophys. Res. Commun.* **373**, 119-124.
Huang, F., Sirinakis, G., Allgeyer, E. S., Schroeder, L. K., Duim, W. C., Kromann, E. B., Phan, T., Rivera-Molina, F. E., Myers, J. R., Irnov, I. et al. (2016). Ultra-high resolution 3D imaging of whole cells. *Cell* **166**, 1028-1040.
Humbert, M. C., Weihbrecht, K., Searby, C. C., Li, Y., Pope, R. M., Sheffield, V. C. and Seo, S. (2012). ARL13B, PDE6D, and CEP164 form a functional network for INPP5E ciliary targeting. *Proc. Natl. Acad. Sci. USA* **109**, 19691-19696.
Iomini, C., Babaev-Khaimov, V., Sassaroli, M. and Piperno, G. (2001). Protein particles in Chlamydomonas flagella undergo a transport cycle consisting of four phases. *J. Cell Biol.* **153**, 13-24.
Iomini, C., Li, L., Mo, W., Dutcher, S. K. and Piperno, G. (2006). Two flagellar genes, AGG2 and AGG3, mediate orientation to light in Chlamydomonas. *Curr. Biol.* **16**, 1147-1153.
Iomini, C., Till, J. E. and Dutcher, S. K. (2009). Genetic and phenotypic analysis of flagellar assembly mutants in Chlamydomonas reinhardtii. *Methods Cell Biol.* **93**, 121-143.
Ivanova, A. A., Caspary, T., Seyfried, N. T., Duong, D. M., West, A. B., Liu, Z. and Kahn, R. A. (2017). Biochemical characterization of purified mammalian ARL13B protein indicates that it is an atypical GTPase and ARL3 guanine nucleotide exchange factor (GEF). *J. Biol. Chem.* **292**, 11091-11108.
Jin, H., White, S. R., Shida, T., Schulz, S., Aguiar, M., Gygi, S. P., Bazan, J. F. and Nachury, M. V. (2010). The conserved Bardet-Biedl syndrome proteins assemble a coat that traffics membrane proteins to cilia. *Cell* **141**, 1208-1219.
Larkins, C. E., Aviles, G. D. G., East, M. P., Kahn, R. A. and Caspary, T. (2011). Arl13b regulates ciliogenesis and the dynamic localization of Shh signaling proteins. *Mol. Biol. Cell* **22**, 4694-4703.
Larkins, C. E., Long, A. B. and Caspary, T. (2012). Defective Nodal and Cerl2 expression in the Arl13b(hnn) mutant node underlie its heterotaxia. *Dev. Biol.* **367**, 15-24.
Lechtreck, K. F. (2015). IFT-cargo interactions and protein transport in cilia. *Trends Biochem. Sci.* **40**, 765-778.
Levi, S., Rawet, M., Kliouchnikov, L., Parnis, A. and Cassel, D. (2008). Topology of amphipathic motifs mediating Golgi localization in ArfGAP1 and its splice isoforms. *J. Biol. Chem.* **283**, 8564-8572.
Mariani, L. E., Bijlsma, M. F., Ivanova, A. I., Suciu, S. K., Kahn, R. A. and Caspary, T. (2016). Arl13b regulates Shh signaling from both inside and outside the cilium. *Mol. Biol. Cell* **27**, 3780-3790.
Miertzschke, M., Koerner, C., Spoerner, M. and Wittinghofer, A. (2014). Structural insights into the small G-protein Arl13B and implications for Joubert syndrome. *Biochem. J.* **457**, 301-311.
Miserey-Lenkei, S., Chalancon, G., Bardin, S., Formstecher, E., Goud, B. and Echard, A. (2010). Rab and actomyosin-dependent fission of transport vesicles at the Golgi complex. *Nat. Cell Biol.* **12**, 645-654.
Mukhopadhyay, S., Wen, X., Chih, B., Nelson, C. D., Lane, W. S., Scales, S. J. and Jackson, P. K. (2010). TULP3 bridges the IFT-A complex and membrane phosphoinositides to promote trafficking of G protein-coupled receptors into primary cilia. *Genes Dev.* **24**, 2180-2193.
Nachury, M. V. (2008). Tandem affinity purification of the BBSome, a critical regulator of Rab8 in ciliogenesis. *Methods Enzymol.* **439**, 501-513.

Nachury, M. V., Seeley, E. S. and Jin, H. (2010). Trafficking to the ciliary membrane: how to get across the periciliary diffusion barrier? *Annu. Rev. Cell Dev. Biol.* **26**, 59-87.
Nesvizhskii, A. I., Keller, A., Kolker, E. and Aebersold, R. (2003). A statistical model for identifying proteins by tandem mass spectrometry. *Anal. Chem.* **75**, 4646-4658.
Nozaki, S., Katoh, Y., Terada, M., Michisaka, S., Funabashi, T., Takahashi, S., Kontani, K. and Nakayama, K. (2017). Regulation of ciliary retrograde protein trafficking by the Joubert syndrome proteins ARL13B and INPP5E. *J. Cell Sci.* **130**, 563-576.
Okai, T., Araki, Y., Tada, M., Tateno, T., Kontani, K. and Katada, T. (2004). Novel small GTPase subfamily capable of associating with tubulin is required for chromosome segregation. *J. Cell Sci.* **117**, 4705-4715.
Pazour, G. J., Agrin, N., Leszyk, J. and Witman, G. B. (2005). Proteomic analysis of a eukaryotic cilium. *J. Cell Biol.* **170**, 103-113.
Piperno, G., Mead, K. and Henderson, S. (1996). Inner dynein arms but not outer dynein arms require the activity of kinesin homologue protein KHP1^{FLA10} to reach the distal part of flagella in *Chlamydomonas*. *J. Cell Biol.* **133**, 371-379.
Price, H. P., Hodgkinson, M. R., Wright, M. H., Tate, E. W., Smith, B. A., Carrington, M., Stark, M. and Smith, D. F. (2012). A role for the vesicle-associated tubulin binding protein ARL6 (BBS3) in flagellum extension in Trypanosoma brucei. *Biochim. Biophys. Acta* **1823**, 1178-1191.
Schwer, B., Erdjument-Bromage, H. and Shuman, S. (2011). Composition of yeast snRNPs and snoRNPs in the absence of trimethylguanosine caps reveals nuclear cap binding protein as a gained U1 component implicated in the cold-sensitivity of tgs1Delta cells. *Nucleic Acids Res.* **39**, 6715-6728.
Sun, Z., Amsterdam, A., Pazour, G. J., Cole, D. G., Miller, M. S. and Hopkins, N. (2004). A genetic screen in zebrafish identifies cilia genes as a principal cause of cystic kidney. *Development* **131**, 4085-4093.
Sung, C.-H. and Leroux, M. R. (2013). The roles of evolutionarily conserved functional modules in cilia-related trafficking. *Nat. Cell Biol.* **15**, 1387-1397.
Thomas, S., Cantagrel, V., Mariani, L., Serre, V., Lee, J.-E., Elkhartoufi, N., de Lonlay, P., Desguerre, I., Munnich, A., Boddaert, N. et al. (2015). Identification of a novel ARL13B variant in a Joubert syndrome-affected patient with retinal impairment and obesity. *Eur. J. Hum. Genet.* **23**, 621-627.
Torres, J. Z., Miller, J. J. and Jackson, P. K. (2009). High-throughput generation of tagged stable cell lines for proteomic analysis. *Proteomics* **9**, 2888-2891.
Ward, H. H., Brown-Glaberman, U., Wang, J., Morita, Y., Alper, S. L., Bedrick, E. J., Gattone, V. H., II, Deretic, D. and Wandinger-Ness, A. (2011). A conserved signal and GTPase complex are required for the ciliary transport of polycystin-1. *Mol. Biol. Cell* **22**, 3289-3305.
Watnick, T. J., Jin, Y., Matunis, E., Kernan, M. J. and Montell, C. (2003). A flagellar polycystin-2 homolog required for male fertility in Drosophila. *Curr. Biol.* **13**, 2179-2184.
Wei, S.-M., Xie, C.-G., Abe, Y. and Cai, J.-T. (2009). ADP-ribosylation factor like 7 (ARL7) interacts with alpha-tubulin and modulates intracellular vesicular transport. *Biochem. Biophys. Res. Commun.* **384**, 352-356.
Zhang, Y., Lam, O., Nguyen, M.-T. T., Ng, G., Pear, W. S., Ai, W., Wang, I.-J., Kao, W. W.-Y. and Liu, C.-Y. (2013). Mastermind-like transcriptional co-activator-mediated Notch signaling is indispensable for maintaining conjunctival epithelial identity. *Development* **140**, 594-605.
Zhang, Q., Li, Y., Zhang, Y., Torres, V. E., Harris, P. C., Ling, K. and Hu, J. (2016). GTP-binding of ARL-3 is activated by ARL-13 as a GEF and stabilized by UNC-119. *Sci. Rep.* **6**, 24534.
Zhou, X. and Anderson, K. V. (2010). Development of head organizer of the mouse embryo depends on a high level of mitochondrial metabolism. *Dev. Biol.* **344**, 185-195.
Zhou, C., Cunningham, L., Marcus, A. I., Li, Y. and Kahn, R. A. (2006). Arl2 and Arl3 regulate different microtubule-dependent processes. *Mol. Biol. Cell* **17**, 2476-2487.